

## Structural and Magnetic Characteristics of $Fe_{72-x}Co_xCr_{28}$ ( $10 < X < 22$ ) Microcrystalline Alloys Prepared by Casting

Elham Ghasemi, Majid Tavoosi, Ali Ghasemi, Mohammad reza Loghman Estarki\*

\* loghman57@gmail.com

Department of Materials Engineering, Malek Ashtar University of Technology, Iran

Received: Desember 2022

Revised: April 2023

Accepted: May 2023

DOI: 10.22068/ijmse.3083

**Abstract:** This study looked at structural and magnetic characteristics of the Fe-Co-Cr system, containing 28 at. % of Cr. Based on the results obtained, the formation of a single  $\alpha$ -phase solid solution in the  $Fe_{72-x}Co_xCr_{28}$  ( $10 < X < 22$ ) system is only possible in alloys containing up to 14 at. % Co and the formation of non-magnetic  $\sigma$  and  $\gamma$  phases in other systems is inevitable. After different processes, the saturation magnetization and coercivity of alloys containing low percentages of Co were estimated to be 137-144 emu/g and 65-110 Oe respectively. The Co content had negligible effect on the magnetic characteristics of  $Fe_{62}Co_{10}Cr_{28}$ ,  $Fe_{60}Co_{12}Cr_{28}$  and  $Fe_{58}Co_{14}Cr_{28}$  alloys.  $Fe_{72-x}Co_xCr_{28}$  ( $10 < X < 22$ ) alloys, with a constant Cr content of about 28 at. %, were outside the miscibility gap in the equilibrium phase diagram, and therefore TMT had no effect on the final magnetic properties.

**Keywords:** Fe-Cr-Co, Casting, Solutioning, Thermo-magnetic treatment.

### 1. INTRODUCTION

Permanent magnets based on Fe-Cr-Co have been known since the 1970s as ductile materials suitable for high-temperature applications due to their high Curie temperature (650°C). Forming facilities, corrosion resistance and appropriate cost-benefit ratio are the main advantages of these alloys compared to Alnico at a similar level of magnetic properties [1-4].

According to the literature, optimal magnetic properties in Fe-Cr-Co alloys are obtained during spinodal transformation [1, 2]. In this process, the  $\alpha$ -phase solid solution is decomposed into Fe-Co-rich ( $\alpha_1$ ) and Cr-rich ( $\alpha_2$ ) coherent spinodal phases [3-10]. However, the formation of FCC  $\gamma$ -phase and tetragonal  $\sigma$ -phase in this system causes a strong weakening of the magnetic properties, and it is necessary to prevent their formation by controlling the composition and annealing process. In this regard, Okada et al. [3] showed that the spinodal decomposition of Fe-Cr alloys is directly related to Co content. Kaneko et al. [8-10] indicated that small amounts of Ti, V, Al, Nb and Si elements in Fe-Cr-Co are effective in promoting regional stability of  $\alpha$ -phase and suppressing harmful  $\gamma$  and  $\sigma$  phases. The results presented by Ahmad [11] and Akbar [12] about the effects of Mo on the alignment of spinodal phases in Fe-Cr-Co alloys and the final magnetic properties of the prepared alloys are among other similar reports in this field.

However, despite the extensive studies available in the field of Fe-Cr-Co alloys, no systematic study on the magnetic properties of alloys containing high percentages of Cr (more than 25 atomic percent) has been presented in the literature. Therefore, in the current research, an attempt has been made to investigate the structural and magnetic characterization of Fe-Co-Cr alloys in the presence of 28 atomic percent of Cr. The effect of replacing Fe with Co on the magnetic properties of these alloys and optimizing the alloy composition and annealing conditions to prevent the precipitation of harmful phases is the main goal of this study.

### 2. EXPERIMENTAL PROCEDURES

In this work, high purity ( $\geq 99.5\%$ ) Fe, Cr and Co ingots were used as raw materials and seven different samples with a nominal composition of  $Fe_{72-x}Co_xCr_{28}$  ( $10 < X < 22$ ) were prepared using the vacuum induction melting method. The dissolution process was carried out at 1200°C for 2 h followed by quenching in cold water. The thermo-magnetic treatment (TMT) process was also done at 580, 610 and 640°C for 40 minutes under an axial magnetic field intensity of 3 kOe. X-ray diffraction (XRD) using a Philips PW3710 diffractometer with Cu K $\alpha$  radiation was used to follow the phase changes of the specimens (step size: 0.05°; time per step: 1 s). The structural characteristics of the prepared samples were



performed using a VEGA-TESCAN-XMU scanning electron microscope (SEM) at an accelerating voltage of 20 kV. The saturation magnetization and coercivity of produced samples were also measured using a vibrating sample magnetometer (VSM) under a maximum applied field of 10 kOe.

### 3. RESULTS AND DISCUSSION

The XRD patterns of different  $\text{Fe}_{72-x}\text{Co}_x\text{Cr}_{28}$  ( $10 < \text{X} < 22$ ) specimens after the casting process are presented in Fig. 1. As can be seen, the structure of as-cast Fe-Co-Cr alloys, at a constant Cr content of 28 at. %, has a direct relation with the percentage of Co and changes from single  $\alpha$ -phase solid solution in  $\text{Fe}_{62}\text{Co}_{10}\text{Cr}_{28}$  to the combination of  $\gamma$  and  $\sigma$  phases in  $\text{Fe}_{50}\text{Co}_{22}\text{Cr}_{28}$  sample. Based on this figure, the single  $\alpha$ -phase solid solution can only be formed in  $\text{Fe}_{62}\text{Co}_{10}\text{Cr}_{28}$  and  $\text{Fe}_{64}\text{Co}_{12}\text{Cr}_{28}$  alloys and the probability of formation of  $\gamma$  and  $\sigma$  non-magnetic phases increases by increasing the cobalt content. This result is consistent with the SEM micrographs of the cast samples presented in Fig. 2. As can be seen, the structure of the sample with low Co content (less than 12 at. %) consists only of the  $\alpha$ -phase solid solution, and with the increase in the content of this element, the undesirable  $\sigma$  and  $\gamma$  phases are deposited on the grain boundaries. In fact, the tetragonal  $\sigma$ -phase has been reported as a stable phase in the Fe-Cr and Fe-Cr-Co systems and this phase appears as Widmanstatten-type precipitates in microstructure, as shown in Fig. 2 (c & d).

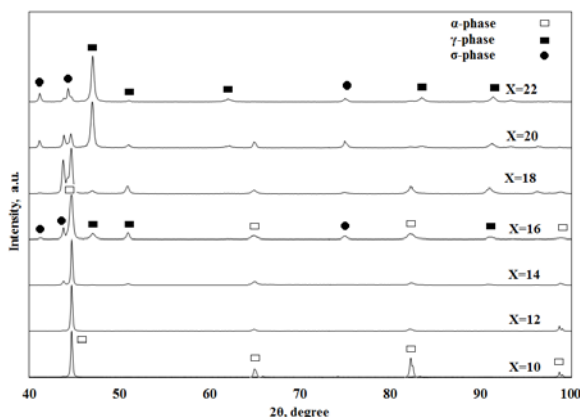


**Fig. 1.** The XRD patterns of as-cast  $\text{Fe}_{72-x}\text{Co}_x\text{Cr}_{28}$  ( $10 < \text{X} < 22$ ) specimens.

The magnetic hysteresis loops and the saturation

magnetization and coercivity of as-cast  $\text{Fe}_{72-x}\text{Co}_x\text{Cr}_{28}$  ( $10 < \text{X} < 22$ ) specimens are presented in Fig. 3 and Table 1. Based on these results several points can be concluded:

1. As the Co content increases, the coercivity increases from 24 to 124 Oe. This manner can be related to the effects of  $\sigma$  and  $\gamma$  precipitates on magnetic field pinning.
2. The saturation magnetization strongly depends on chemical composition and gradually decreases from 169 to 14 emu/g by increasing Co content.
3. The sample containing 10 at. % of Co has a maximum value of saturation magnetization of about 169 emu/g. This high value of  $M_s$  can be related to the formation of a single  $\alpha$  ferromagnetic phase in this sample.
4.  $\text{Fe}_{52}\text{Co}_{20}\text{Cr}_{28}$  and  $\text{Fe}_{50}\text{Co}_{22}\text{Cr}_{28}$  alloys show minimum  $M_s$  values (about 14–22 emu/g) as a result of precipitation of non-magnetic  $\sigma$  and  $\gamma$  phases in these samples. In fact, saturation magnetization is related to the number of magnetic moments per unit volume, and the precipitation of non-magnetic phases against the ferromagnetic phase is the main reason for the decrease of  $M_s$  value with the increase of Co content.

XRD patterns of different  $\text{Fe}_{72-x}\text{Co}_x\text{Cr}_{28}$  ( $10 < \text{X} < 22$ ) samples after the solutioning process at  $1200^\circ\text{C}$  are presented in Fig. 4. Based on this figure, the diffraction patterns of  $\text{Fe}_{62}\text{Co}_{10}\text{Cr}_{28}$ ,  $\text{Fe}_{60}\text{Co}_{12}\text{Cr}_{28}$  and  $\text{Fe}_{58}\text{Co}_{14}\text{Cr}_{28}$  alloys after the solutioning process only include three peaks corresponding to  $\alpha$ -phase solid solution with BCC structure and lattice parameter of about 0.288 nm. The presented SEM micrographs of these alloys in Fig. 5 also confirm this result. As can be seen, the microstructures of the discussed samples only include relatively equiaxed grains of the  $\alpha$ -phase with average sizes of about  $218 \mu\text{m}$ , and no sign of the formation of other phases can be seen in the images. Linear micro-chemical analysis of the discussed samples across the grain boundaries in Fig. 6 shows a uniform distribution of Fe, Cr and Co elements throughout the structure. As can be seen in Fig. 4, the diffraction patterns of samples with Co content greater than 14 at. %, in addition to the peaks related to the  $\alpha$ -phase, include narrow peaks corresponding to undesirable  $\sigma$  and  $\gamma$  phases. This result indicates that the formation of a single  $\alpha$ -phase solid solution is possible only in alloys containing less than 14 at. % of Co.

The magnetic hysteresis loops and the saturation magnetization and coercivity of as-homogenized

$\text{Fe}_{72-x}\text{Co}_x\text{Cr}_{28}$  ( $10 < X < 22$ ) specimens are presented in Fig. 7 and Table. 2.

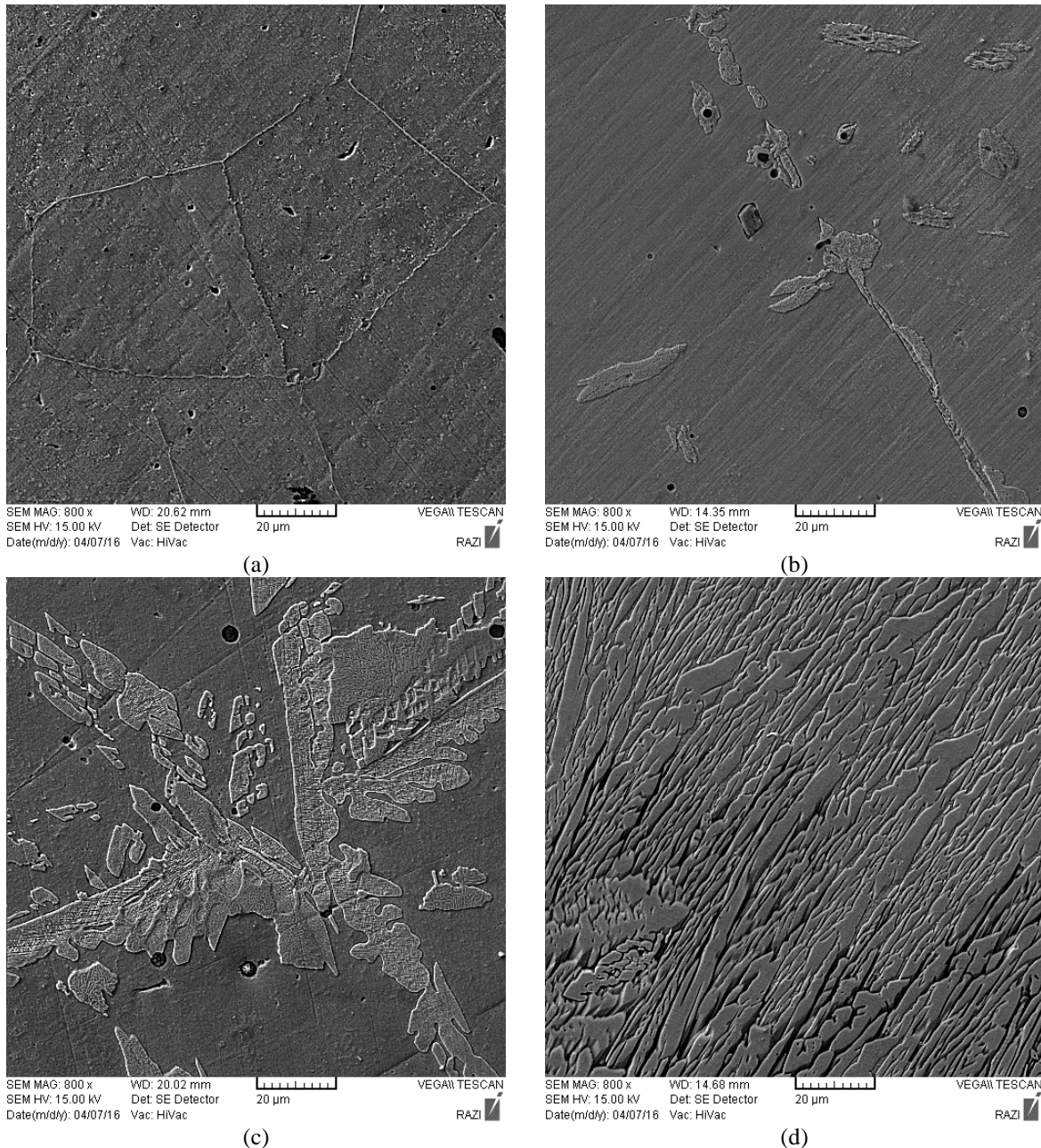
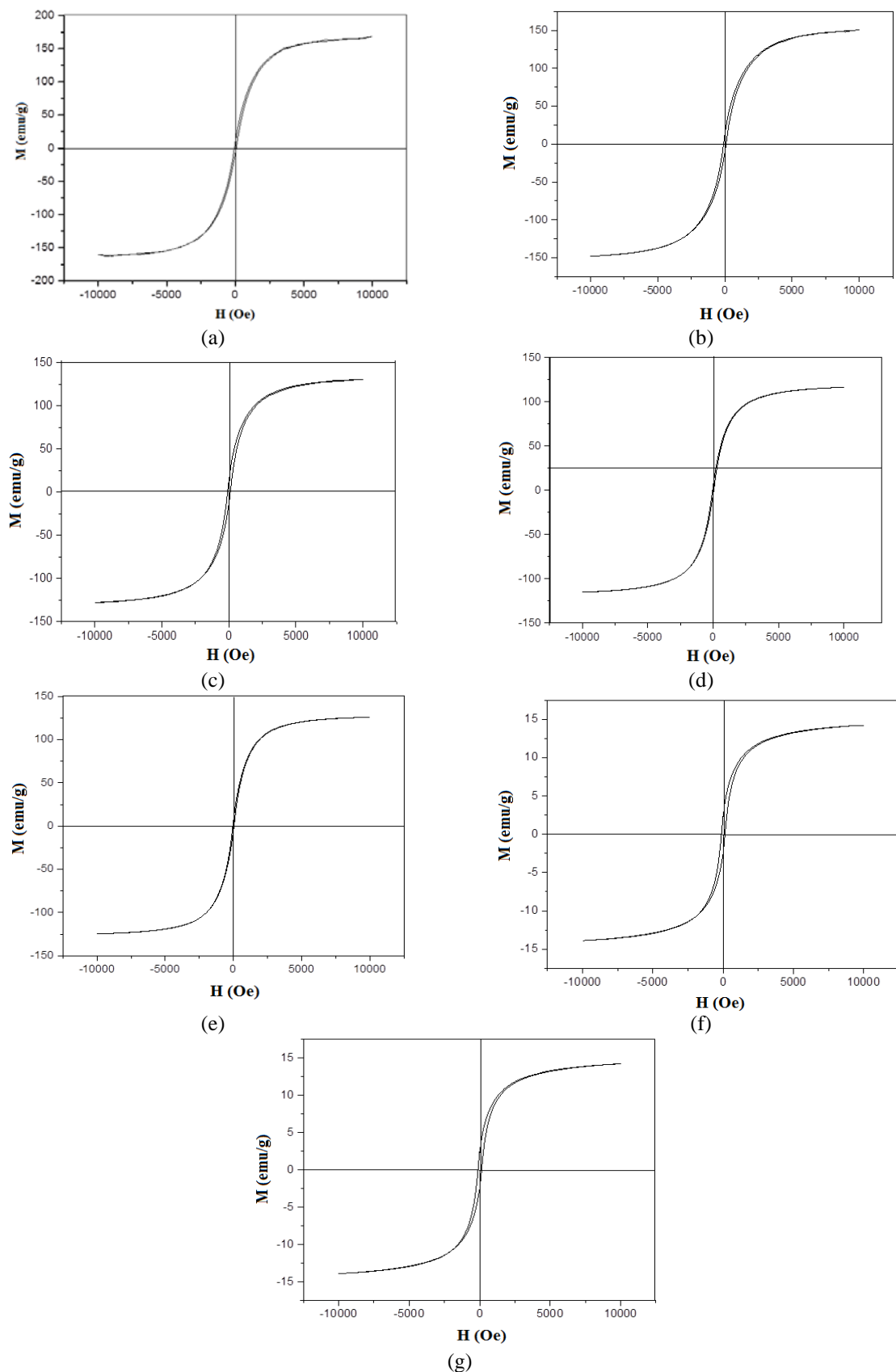


Fig. 2. The SEM micrographs of as-cast  $\text{Fe}_{72-x}\text{Co}_x\text{Cr}_{28}$  specimens; a)  $X = 10$ , b)  $X = 14$ , c)  $X = 18$  and d)  $X = 22$ .

**Table 1.** The saturation magnetization and coercivity values of as-cast  $\text{Fe}_{72-x}\text{Co}_x\text{Cr}_{28}$  specimens

X	Hc (Oe)	Ms (emu/g)
10	24	169
12	38	150
14	41	130
16	89	116
18	100	115
20	110	22
22	124	14



**Fig. 3.** The magnetic hysteresis loops of as-cast  $\text{Fe}_{72-x}\text{Co}_x\text{Cr}_{28}$  specimens; a)  $X=10$ , b)  $X=12$ , c)  $X=14$ , d)  $X=16$ , e)  $X=18$ , f)  $X=20$  and g)  $X=22$ .

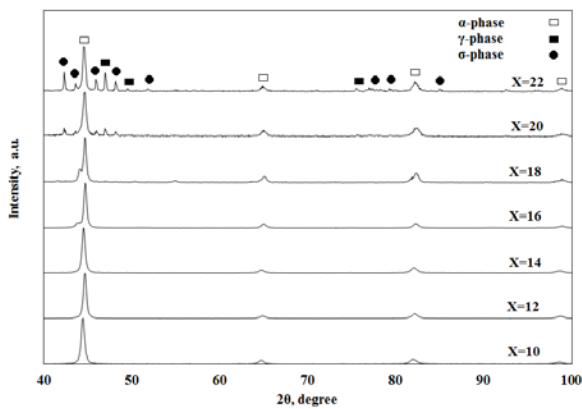


**Fig. 4.** The XRD patterns of  $\text{Fe}_{72-x}\text{Co}_x\text{Cr}_{28}$  ( $10 < \text{X} < 22$ ) specimens after solutioning process at  $1200^\circ\text{C}$  for 2 h.

As can be seen, there is no significant difference between the magnetic properties of samples containing less than 14 at. % of Co as a result of same structural characteristics of these specimens. In contrast, by increasing the Co content, the coercivity and magnetization saturation increase and decrease, respectively. In fact, the coercivity strongly depends on the movement of the magnetic field wall. Based on structural investigations, the presence of σ and γ phases along with α-phase in samples containing a higher percentage of Co causes the domain walls to lock and slow down, which leads to an increase in coercivity [12-15].

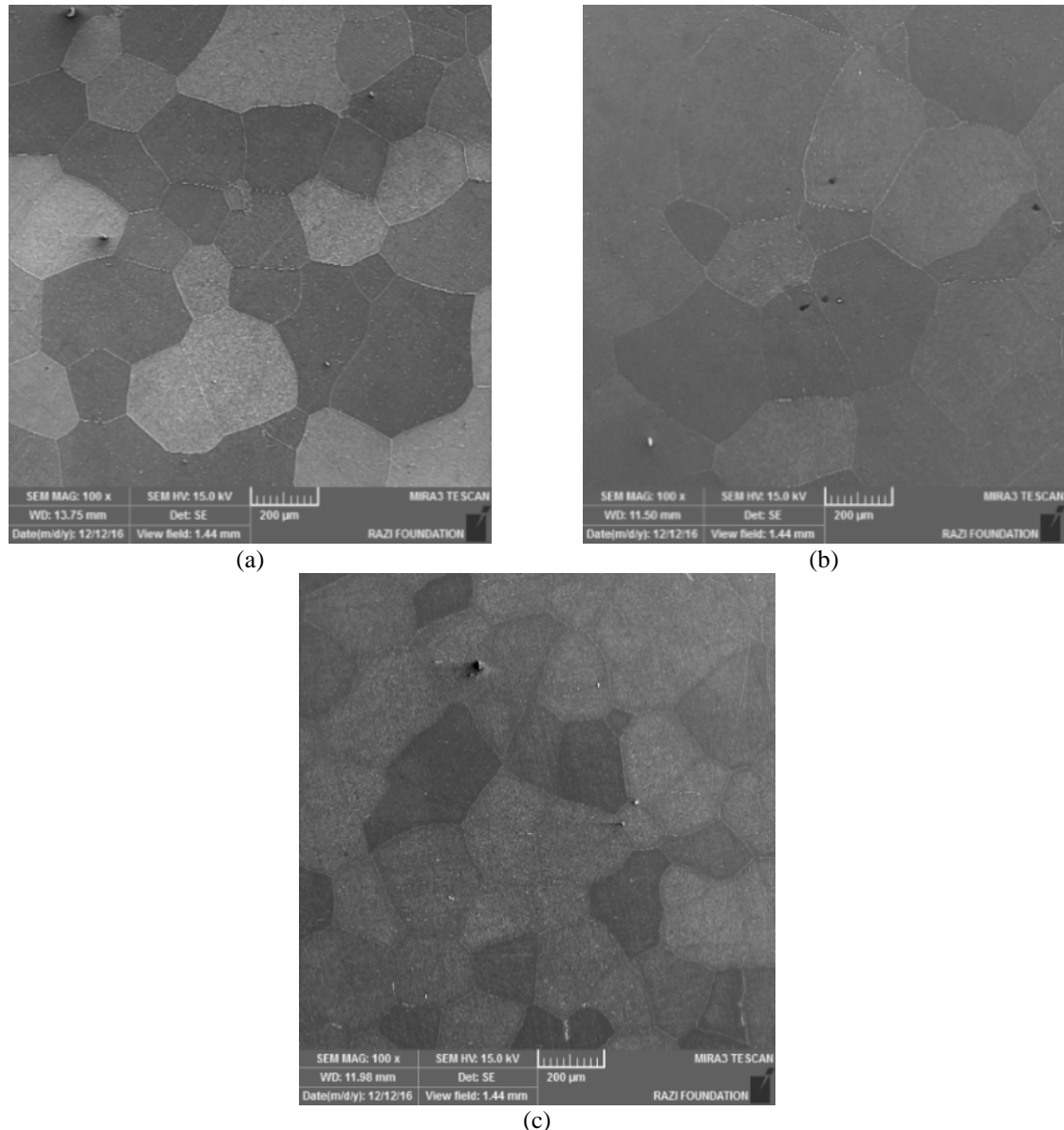


**Fig. 5.** The SEM micrographs of a)  $\text{Fe}_{62}\text{Co}_{10}\text{Cr}_{28}$ , b)  $\text{Fe}_{60}\text{Co}_{12}\text{Cr}_{28}$  and c)  $\text{Fe}_{58}\text{Co}_{14}\text{Cr}_{28}$  after the solutioning process at  $1200^\circ\text{C}$  for 2 h.

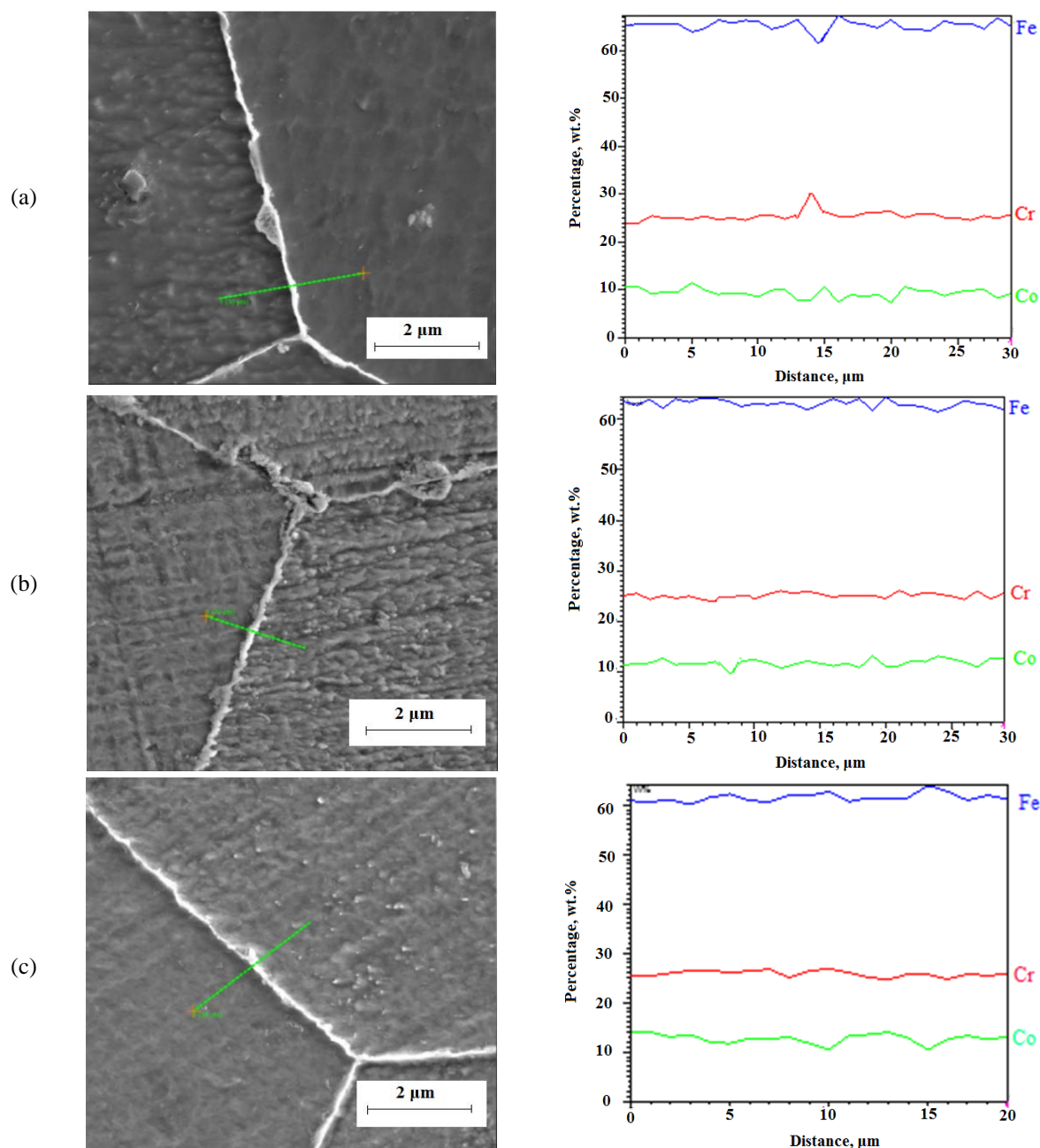


**Fig. 6.** Liner micro-chemical analysis of a)  $\text{Fe}_{62}\text{Co}_{10}\text{Cr}_{28}$ , b)  $\text{Fe}_{60}\text{Co}_{12}\text{Cr}_{28}$  and c)  $\text{Fe}_{58}\text{Co}_{14}\text{Cr}_{28}$  across the grain boundaries after the solutioning process at  $1200^\circ\text{C}$  for 2 h.

**Table 2.** The saturation magnetization and coercivity values of  $\text{Fe}_{72-x}\text{Cox}\text{Cr}_{28}$  specimens after solutioning process at  $1200^\circ\text{C}$  for 2 h.

X	Hc (Oe)	Ms (emu/g)
10	61	141
12	64	144
14	66	142
16	100	92
18	114	47
20	116	32
22	120	27

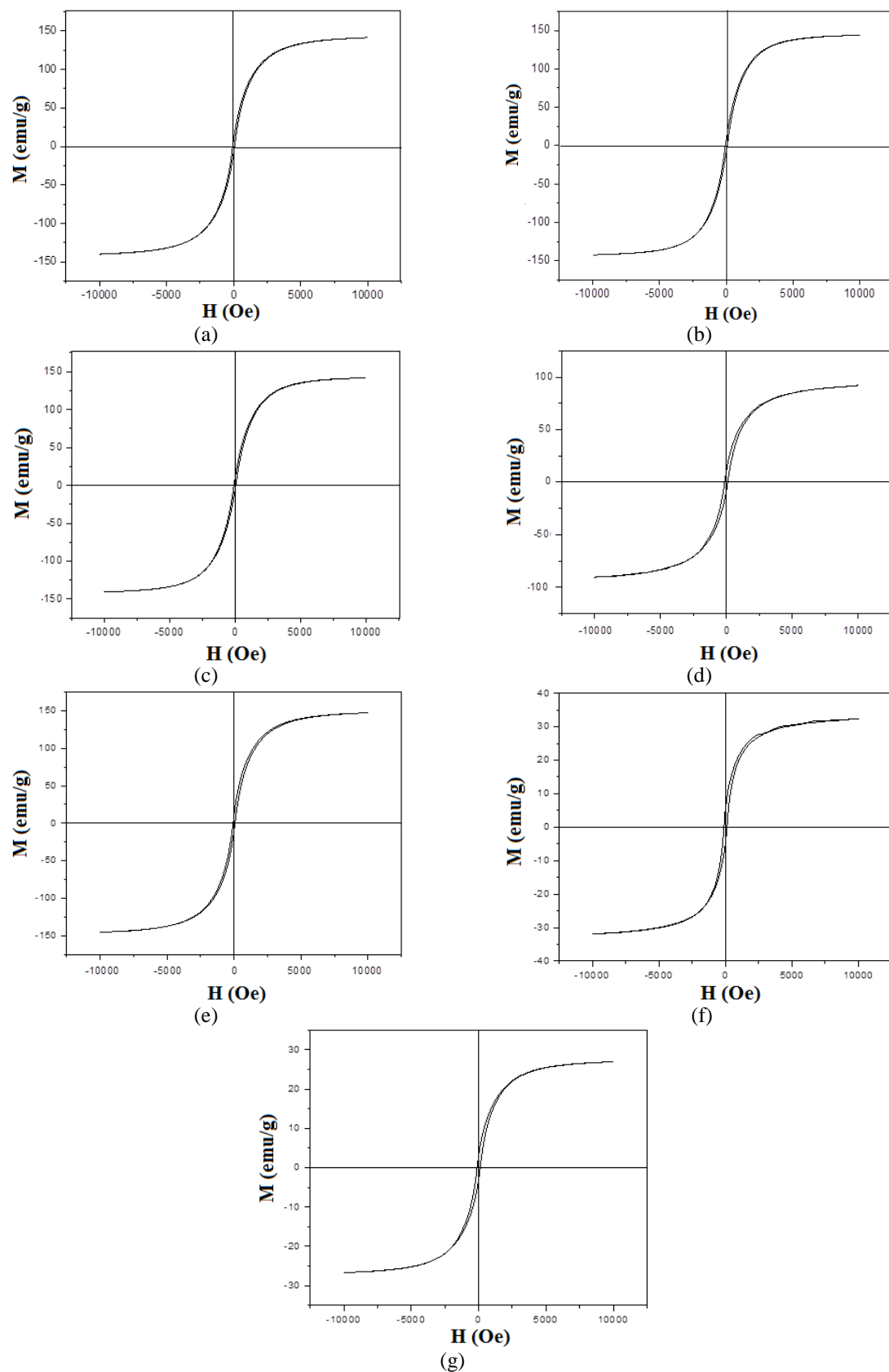


**Fig. 7.** The magnetic hysteresis loops of  $\text{Fe}_{72-x}\text{Co}_x\text{Cr}_{28}$  specimens after solutioning process at  $1200^\circ\text{C}$  for 2 h; a)  $X = 10$ , b)  $X = 12$ , c)  $X = 14$ , d)  $X = 16$ , e)  $X = 18$ , f)  $X = 20$  and g)  $X = 22$ .

In addition, the precipitation of non-magnetic  $\sigma$  and  $\gamma$  phases in these samples is the main reason for the decrease in saturation magnetization with increasing Co content.

According to the presented results about the obtained samples from the casting and solutioning process, among all the samples, only Fe<sub>62</sub>Co<sub>10</sub>Cr<sub>28</sub>, Fe<sub>60</sub>Co<sub>12</sub>Cr<sub>28</sub> and Fe<sub>58</sub>Co<sub>14</sub>Cr<sub>28</sub> alloys (with single  $\alpha$ -phase) were selected to investigate the effect of the TMT on final magnetic properties. It is known that, the obtained magnetic properties of Fe-Cr-Co alloys after

TMT are sensitive to the different processing parameters such as temperature, holding time and applied magnetic field intensity [1-5, 16-20]. In this work, all the processing parameters were kept constant and the effects of TMT temperature on magnetic behaviors of different alloys were investigated. In this regards, the magnetic hysteresis loops and the saturation magnetization and coercivity of Fe<sub>62</sub>Co<sub>10</sub>Cr<sub>28</sub>, Fe<sub>60</sub>Co<sub>12</sub>Cr<sub>28</sub> and Fe<sub>58</sub>Co<sub>14</sub>Cr<sub>28</sub> alloys after thermo-magnetic treatments at 580, 610 and 640°C are presented in Tables. 3 to 5.

**Table 3.** The magnetic hysteresis loops and magnetic properties of Fe<sub>62</sub>Co<sub>10</sub>Cr<sub>28</sub>, Fe<sub>60</sub>Co<sub>12</sub>Cr<sub>28</sub> and Fe<sub>58</sub>Co<sub>14</sub>Cr<sub>28</sub> alloys after TMT process at 580°C.

X	Hysteresis loop	Hc (Oe)	Ms (emu/g)
10		67	140
12		69	144
14		65	137

**Table 4.** The magnetic hysteresis loops and magnetic properties of  $\text{Fe}_{62}\text{Co}_{10}\text{Cr}_{28}$ ,  $\text{Fe}_{60}\text{Co}_{12}\text{Cr}_{28}$  and  $\text{Fe}_{58}\text{Co}_{14}\text{Cr}_{28}$  alloys after TMT process at  $610^\circ\text{C}$ .

X	Hysteresis loop	Hc (Oe)	Ms (emu/g)
10		74	144
12		75	136
14		80	144

As can be seen, all investigated samples have similar soft magnetic properties with magnetization saturation of about 137-144 emu/g. The coercivity values after TMT are also low (65-110 Oe,) and far from the values predicted by theoretical estimates. There is no significant difference between samples processed at different TMT temperatures and resulting magnetic properties are very similar to the samples before

process. In other words, the TMT had no effect on the magnetic properties of the studied compounds. However, the optimal magnetic properties of Fe-Cr-Co alloys with miscibility gap can be obtained only during spinodal decomposition. It is clear that this process cannot occur by choosing a compound outside the miscibility gap in the equilibrium phase diagram. It seems that  $\text{Fe}_{72-x}\text{Co}_x\text{Cr}_{28}$  ( $10 < X < 22$ ) alloys with

constant Cr content of about 28 at. % are outside the miscibility gap in the equilibrium phase diagram, and TMT has no effect on the final

magnetic properties. Consequently, this alloying composition is not recommended for making permanent magnets in Fe-Cr-Co system.

**Table 5.** The magnetic hysteresis loops and magnetic properties of  $\text{Fe}_{62}\text{Co}_{10}\text{Cr}_{28}$ ,  $\text{Fe}_{60}\text{Co}_{12}\text{Cr}_{28}$  and  $\text{Fe}_{58}\text{Co}_{14}\text{Cr}_{28}$  alloys after TMT process at  $640^\circ\text{C}$ .

X	Hysteresis loop	Hc (Oe)	Ms (emu/g)
10		90	137
12		97	143
14		109	142

#### 4. CONCLUSIONS

The structural and magnetic properties of the Fe-Co-Cr system, in the presence of a high percentage of Cr (28 at. %) were investigated. The

results showed that the formation of single  $\alpha$ -phase solid solution in the  $\text{Fe}_{72-x}\text{Co}_x\text{Cr}_{28}$  ( $10 < X < 22$ ) system was only possible in alloys containing up to 14 at. % Co and the formation of non-magnetic  $\sigma$  and  $\gamma$  phases

at higher Co contents was inevitable. Saturation magnetization and coercivity of alloys containing low percentages of Co after casting, solutioning and TMT processes were similar and were estimated to be 137-144 emu/g and 65-110 Oe, respectively. The Co content and thermomagnetic treatment had negligible effect on magnetic characteristics of Fe<sub>62</sub>Co<sub>10</sub>Cr<sub>28</sub>, Fe<sub>60</sub>Co<sub>12</sub>Cr<sub>28</sub> and Fe<sub>58</sub>Co<sub>14</sub>Cr<sub>28</sub> alloys. Fe<sub>72-x</sub>Co<sub>x</sub>Cr<sub>28</sub> (10<X<22) alloys with a high Cr content (28 at. %) were outside the miscibility gap in the equilibrium phase diagram, and therefore TMT had no effect on the final magnetic properties.

## REFERENCES

- [1] Jin, S., and G. Chin. "Fe-Cr-Co magnets." IEEE transact. Magnet. 1987, 23, no. 5, 3187-3192.
- [2] Ushakova, Olga, and Raisa Malinina. "Structure and magnetic properties of nanocrystalline Fe-Cr-Co alloys for permanent magnets." In Solid State Phenomena, Trans Tech Publications Ltd, 2012, 190, 238-242.
- [3] Okada, M., Thomas, G., Homma, M., & Kaneko, H. "Microstructure and magnetic properties of Fe-Cr-Co alloys." IEEE Transact. Magnet. 1978, 14, 245-252.
- [4] Kubota, T., Wakui, G., & Itagaki, M. "Hysteresis motor using magnetically anisotropic Fe-Cr-Co magnet." IEEE Transactions on Magnetics, 1998, 34, 3888-3896.
- [5] Ahmad, Z., A. Ul Haq, S. W. Husain, A. Ali, and T. Abbas. "Influence of Ti content on magnetic and microstructural properties of Fe-28Cr-15Co-3.5 Mo permanent magnets." J. Magnet. Magnet. Mat. 2003, 257, 397-402.
- [6] Sugimoto, S., M. Okada, and M. Homma. "The enhancement of the magnetic properties of Fe-Cr-Co-Mo polycrystalline permanent magnet alloys by cold rolling and annealing." J. Appl. Phys. 1988, 63, 3707-3709.
- [7] Sun, X. Y., C. Y. Xu, L. Zhen, L. X. Lu, and L-C. Qin. "Spinodal decomposition in Fe-25Cr-12Co-1Si alloy under a 100 kOe magnetic field." J. Magnet. Magnet. Mat. 2006, 306, 69-72.
- [8] Kaneko, H., M. Homma, T. Fukunaga, and M. Okada. "Fe-Cr-Co permanent magnet alloys containing Nb and Al." IEEE Transacti. Magnet.1975, 11, 1440-1442.
- [9] Kaneko, H., M. Homma, and T. Minowa. "Effect of V and V+ Ti additions on the structure and properties of Fe-Cr-Co ductile magnet alloys." IEEE Transacti. Magnet. 1976, 12, 977-979.
- [10] HKaneko, H., M. Homma, K. Nakamura, M. Okada, and G. Thomas. "Phase diagram of Fe-Cr-Co permanent magnet system." IEEE Transacti. Magnet. 1977, 13, 1325-1327.
- [11] Ahmad, Z., and A. Ul Haq. "Texture, microstructure and magnetic properties of Fe-28Cr-15Co-3.5 Mo permanent magnet." J. Magnet. Magnet. Mat.2004, 321, 325-329.
- [12] Akbar, S., Awan, M. S., Aleem, M. A., & Sarwar, M. N. "Development of Mo containing Fe-Cr-Co permanent magnets by modified single step thermomagnetic treatment." IEEE Transacti. Magnet. 2014, 501-4.
- [13] Rastabi, R. A., Ghasemi, A., Tavoosi, M., & Sodaee, T. "Magnetic characterization of nanocrystalline Fe<sub>80-x</sub>Cr<sub>x</sub>Co<sub>20</sub> (15≤x≤35) alloys during milling and subsequent annealing." J. Magnet. Magnet. Mat. 2016, 416, 174-180.
- [14] Rastabi, R. A., Ghasemi, A., Tavoosi, M., & Ramazani, M. "Magnetic features of Fe-Cr-Co alloys with tailoring chromium content fabricated by spark plasma sintering." J. Magnet. Magnet. Mat. 2017, 426 744-752.
- [15] Cullity, B. D., & Graham, C. D. Introduction to magnetic materials. John Wiley & Sons, 2011.
- [16] Stoner, E. C., & Wohlfarth, E. P. "A mechanism of magnetic hysteresis in heterogeneous alloys." Philosophical Transactions of the Royal Society of London. Series A, Mathemati. Phys. Sci., 1948, 240, 599-642.
- [17] Jacobs, I. S., and C. P. Bean. "An approach to elongated fine-particle magnets." Phys. Rev. 1955, 100, 1060.
- [18] Ghasemi, E., Ghasemi, A., Hadi, M., Sadeghi, M., Hashemi, S. H., Tavoosi, M., & Gordani, G. R. "Effect of cobalt

- doping on structural and magnetic characterization of nanocrystalline  $\text{Fe}_{72-x}\text{Co}_x\text{Cr}_{28}$  ( $10 < \text{X} < 22$ ) alloys." *J. Magnet. Magnet. Mat.* 2018, 468, 56-64.
- [19] Khan, I. U., Tirth, V., Algahtani, A., Khan, R., Sohail, M., Ali, A., & Irshad, K. "Optimization of Single  $\alpha$ -Phase for Promoting Ferromagnetic Properties of 44Fe–28Cr–22Co–3Mo–1Ti–2V Permanent Magnet with Varying Co Concentration for Energy Storage." *Mat.* 2022 15, 2344.
- [20] Tweddle, D., A. Koenig, P. Nakarmi, A. M. Leary, R. D. Noebe, T. Mewes, C. Mewes, and G. B. Thompson. "Phase evolution and magnetic properties of a Co-rich multi-component magnetic nanocomposite film." *J. Alloys Compds.* 2022, 903, 163782.